Mustansiriyah Journal of Pure and Applied Sciences, Print ISSN: 2957-9910. Online ISSN: 2957-9929, Vol. 4, No. 3, 2026, Pages 105-118
DOI: 10.47831/mjpas.v4i3.453

MJPAS

MUSTANSIRIYAH JOURNAL OF PURE AND APPLIED SCIENCES
Journal homepage:
https://mjpas.uomustansiriyah.edu.iq/index.php/mjpas

RESEARCH ARTICLE - PHYSICS

Simulation Study for Optical Sensing Based on Self-Mixing Effect

Hawraa H. Khalaf [1,2], Ayser A. Hemed [1]

[1] Department of Physics, College of Education, Mustansiriyah University, Baghdad-Iraq
[2] College of Remote Sensing and Geophysics, Alkarkh University of Science, Baghdad – Iraq
[*] Corresponding author: hawraahussein@uomustansiriyah.edu.iq

Article Info.

Article history:

Received
16 June 2025

Accepted
1 September 2025

Publishing
30 September 2026

Abstract

This simulation investigates optical feedback (self-mixing) in a single-longitudinal-mode laser cavity, which is crucial for a novel interrogation technique for a fiber Bragg grating (FBG)-based temperature sensor. In essence, the article explores a new sensory system through an intriguing and attractive technique. In this system, the signal used for sensing in the channel sent to the medium is inconvenient. It is susceptible, such that any slight change in medium temperature elicits a significant response in the back-reflected sensing signal. Accordingly, the sensing accuracy rapidly increases compared to traditional fiber sensors. The sensor system comprises a laser diode (DFB) integrated with a photodiode connected to an FBG for temperature measurement. The grating structure resonantly reflects a minor portion of the injected light wave and reenters the LD cavity. This study was performed within a weak feedback regime, with a measure feedback parameter: C = 0.2, along with a temperature range of 10 °C to 100 °C with incremental variations. The obtained results show a robust linear correlation between the center wavelength shift (λ) and temperature fluctuations. The analysis results show a wavelength shift of 100 µm for every 10°C change. The resulting sensitivity is 0.53 pm/°C. The results also show a bandwidth expansion to 11.4 GHz at 60 °C.

The official journal published by the College of Education at Mustansiriyah University

Keywords: Fiber Bragg grating (FBG), Self-mixing interferometry (SMI), Temperature, Chaoticity, Laser Diode.

Introduction

Self-mixing interferometry (SMI) occurs when a portion of a laser beam aimed at a distant target is backscattered, disturbing the internal optical field. Consequently, fluctuations in laser parameters, including laser wavelength and output optical power (OOP), emerge due to alterations to the optical path length between the laser and the distant target [1]. As an attractive indirect sensing technique, the self-mixing has drawn significant attention from researchers in the past few years due to its cost-effectiveness and flexibility in optical equilibrium. Numerous SMI-based sensing applications have been recorded [2], including measuring diverse metrological parameters, velocity, vibration, and displacement [3]. Unlike traditional interferometers based on Michelson's structure, this newly developed interferometer is much better because the interferometric signal is already in the laser beam and is not produced by the interference of two beams from separate paths. This means that the optical component that separates the reference path from the measurement path is unnecessary [4]. The target reflectivity significantly influences SM behavior. Fiber Bragg gratings (FBGs) can be utilized in SM systems as external reflectors. The SM model, typically constructed for single-cavity lasers with a reflective target, is nearly perfect at weak and extremely weak feedback conditions, where sensing devices perform. As the optical feedback (OFB) strength increases, the entire system becomes bistable in a modestly higher feedback domain and becomes more unstable as the feedback level goes up. In this case, the standard SM model doesn't work because the large back reflection causes chaotic activity inside the laser cavity [5], [6] ,[7]. The FBGs behave as transducers for various sensing applications due to their flexibility in both Λ (grating pitch) and n_{eff} (effective index of the grating). In response to external disturbances, such as the variations due to the temperature and external strains. Light propagates through the core of an optical fiber, which integrates a Bragg grating. The multiple reflections from this grating create a stable sensing mechanism [8], [9]. When the FBG is exposed to temperature or strain, it will experience a wavelength shift λ, enabling its "center wavelength" to shift to a lower or higher value. The direction and intensity of the change are proportional to the fluctuations in temperature or external strain [10], [11], [12]. A fiber Bragg grating with a Bragg wavelength of 1550 nm typically has a temperature sensitivity of approximately 10 pm/°C and a strain sensitivity of 1 pm/μstrain, respectively [13],[14],[15],[16]. The sensing mechanism of an SMI system depends on the self-mixing effect of a laser. Like in Michelson interferometry, the laser intensity in an SMI system changes because of interference patterns formed when an electromagnetic wave inside the cavity interacts with an incoming electromagnetic wave that is sent back into the laser cavity, following external influences. The exterior tension (temperature or strain) changes the trajectory of light, generating an SMI signal [17],[18]. (OFB) A signal to a laser cavity may induce chaotic instability in the LD output. An optical feedback signal can reduce the balance of the laser medium's carrier–photon interaction, making the laser intensity unstable. Several nonlinear dynamical phenomena, including bistability, instabilities, and coherent collapse, are detected based on the strength of the (OFB) signal [19],[20].

This simulation presents a new method employing the self-mixing phenomenon to detect the center wavelength shifts due to changing temperature fluctuations in a fiber Bragg grating (FBG). The FBG is directly attached to a distributed feedback (DFB) LD setup that includes an optical spectrum analyzer (OSA), a photodiode (PD), and a power meter. The sensor layout is much optimized, with the laser diode performing as a transmitter and detector simultaneously.

Theoretical Analysis

A typical SMI system comprises an LD, a photodiode (PD), and a target (mirror, lens, etc.). The target offers an external cavity for the laser, and when it moves across the light beam, the photodetector on the back of the LD may detect and evaluate a change in the laser power that is released. An SMI signal, which offers details about the flexibility of the target and the SL itself, has been identified from this modulated power. As seen in Fig. 1 [21], the SMI model often evolved from the traditional three-mirror model, which included the target reflection coefficient r_3, in addition to the facet reflection coefficients r_1 and r_2.

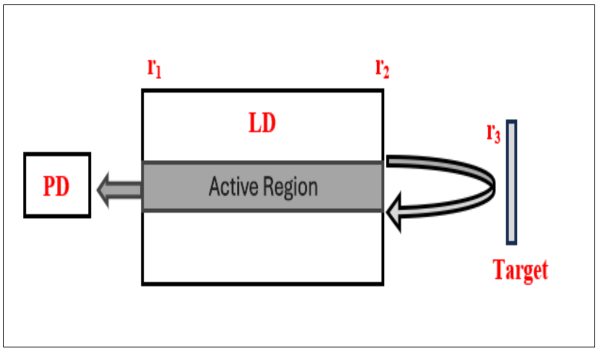

Fig. 1: Typical self-mixing configuration regarding an LD.

A comprehensive investigation of the (LD) with OFB can be conducted employing the equations first derived by Lang and Kobayashi [22],[19],[23] that indicates the association between the amplitude of the electric field $E_0(t)$, and optical phases $\emptyset(t)$, carrier density in the active layer $N(t)$:

$$\frac{dE_o(t)}{dt} = \frac{1}{2}[G_N(N(t) - N_O) - 1/\tau_P]E_O(t) + \frac{K}{\tau_L}E_O(t-\tau) \times \cos[\omega_o\tau + \emptyset(t) - \emptyset(t-\tau)] \dots\dots (1)$$

$$\frac{d\emptyset(t)}{dt} = \frac{\alpha}{2}G_N[N(t) - N_T] - \frac{K}{\tau_L}\frac{E_0(t-\tau)}{E_o(t)}\sin[\omega_o\tau + \emptyset(t) - \emptyset(t-\tau)] \dots . (2)$$

$$\frac{dN(t)}{dt} = R_P - \frac{N(t)}{\tau_s} - G_N[N(t) - N_0]E_O^2(t) \dots\dots (3)$$

where: N_T is the threshold carrier density, τ_L is the intracavity round-trip time, N_O is the carrier density at transparency, G_N is the modal gain, $E_O^2(t)$ is the photon density in the laser cavity, α is the linewidth enhancement factor, τ_s the carrier lifetime, τ is the external cavity round-trip time, τ_s the carrier lifetime, τ_P the photon lifetime, ω_o is the angular frequency of LDs, K is the feedback parameter, R_P the electric pumping term. In the OptiSystem 21 software, a theoretical model using a spatially averaged multimode method is included in the DFB laser icon [24]. The final set of coupled first-order differential equations is numerically integrated using a Runge–Kutta technique using values from Table 1[25].

Table 1. Parameters for numerical analysis of free-running laser diodes.

Laser Parameter	Symbol	Value
emission wavelength	λ	1550 nm
differential gain coefficient	σ_g	$1 \times 10^{-16} cm^2$
group velocity	v_g	$8.5 \times 10^9 \frac{cm}{s}$
active layer volume	V	$1.8 \times 10^{-10} cm^3$
linewidth enhancement factor	α	5
carrier lifetime	τ_s	$1.86 \times 10^{-9} s$

Back-reflected light interferes with the cavity's existing light due to the optical delayed feedback. The emitted power fluctuates as the pump current remains constant, influenced by the phase and delay of the back-reflected light, which affects the LD threshold condition. Any change in the threshold means that the actual LD carrier density is adjusted; as a result, the wavelength emitted by the LD experiencing back-reflections is also changed a little. The self-mixing effect includes a variation in carrier density, with its characteristic time typically comparable to the carrier lifetime, specifically in the sub-nanosecond range [26]. Finding an analytical steady-state solution useful for sensing applications is straightforward and offers the basic formula for the power emitted by the LD as follows [27]:

$$P(\emptyset) = P_0[1 + m \cos \emptyset_F] \quad \ldots\ldots (4)$$

$$\emptyset_F = \emptyset_O - C \sin(\emptyset_F + arctan\alpha) \ldots\ldots (5)$$

Eq. 4 is the SMI system's power equation, where P_0 is the power released by the unperturbed LD, and m is the modulation index. The phase equation of the SMI is shown in Eq. 5, where C refers to the optical feedback intensity factor and α indicates the LD linewidth enhancement factor. The phase signals of the laser without optical feedback are represented by $\emptyset_O$. Factor C, often known as the feedback parameter, is an essential variable for SMI systems that describes SMI signals. The C parameter plays an important role because it uses the following inequalities to differentiate between various feedback regimes [28],[29].

$$C = \frac{ks\sqrt{1+\alpha^2}}{L_{las} n_{las}} \quad \ldots \quad \ldots . (6)$$

where L_{las} is the LD cavity length, α is the LD linewidth enhancement factor, n_{las} is the cavity refractive index, and κ is given by: $k = \frac{\varepsilon}{\sqrt{A}} \frac{1-R_2}{\sqrt{R_2}}$, where A is the total optical power attenuation in the external cavity, and $\varepsilon \leq 1$ accounts for a mismatch between the reflected and the lasing modes, and R_2 is the LD output facet power reflectivity.

$$\left.\begin{array}{c} C \ll 1 \ \rightarrow very\ weak\ OFB \\ 0.1 < C < 1 \ \rightarrow \ weak\ OFB \\ 1 < C < 4.6 \ \rightarrow \ moderate\ OFB \\ C > 4.6 \ \rightarrow \ strong\ OFB \end{array}\right\} \quad \ldots \ldots (7)$$

Regime I (weak feedback): Limited influence and weak feedback. The electric field amplitude's feedback level is less than 0.01%. Depending on the feedback percentage, the laser oscillation's linewidth can either become wide or narrow. Regime II: Minor, yet significant impacts. The feedback level is under 0.1%. The generation of exterior modes induces mode mixing between external and internal patterns. Regime III: This is a limited region with a feedback level of approximately 0.1%. By reducing the mode-hopping noise, the laser can oscillate with a small linewidth. Regime IV: This regime is distinguished by a moderate feedback level of approximately 1%. When the relaxation oscillation is undamped, the laser linewidth significantly widens. The laser behaves chaotically and alternates between unstable oscillations and a condition of coherence-collapse. The noise rate grows substantially in this kind of circumstance. Regime V: This strong feedback regime is characterized by a higher than 10% feedback level. The internal and external cavities operate as one cavity, leaving the laser oscillating in a singular pattern. The laser linewidth is significantly reduced [19],[30].

Simulation Set-up

Following the above theoretical model, a theoretical structure has been established to clarify the effect of temperature on the sensitivity of self-mixing interferometry (SMI). To realize the SM principle for this theoretical simulation, two cavities, internal (laser cavity) and external (FBG), must be established. When optical feedback is used, the light that leaves the laser is reflected by an external reflector, which in this case is an FBG, and then travels back along the same optical path to the laser cavity. Modulation of the laser's inner light by the feedback light conveying the external cavity's information, that constructed from FBG and a virtual inner laser cavity, causing changes in the laser's amplitude, phase, polarization, and other properties. In this study, the phase change resulting from the temperature effect was relied upon as an external disturbance. The experimental setup is illustrated schematically in Fig. 2. There are two twin (identical) DFBL devices similar in all operating parameters, in addition to the device model in software. Duplication is to overcome limitations presented in the Optisystem 21 software when subjecting LD to self-mixing. A portion of an optical signal generated by the LD (DFB1) is routed to an optical power meter and an optical spectrum analyzer (OSA) to measure the free-running optical power of the LD. The optical signal arrives at the FBG, which is exposed to temperatures between (10 – 100) °C. Due to the unique spectrum reflection characteristics of the FBG, the feedback to the DFB is 0.99. Wavelength shifts in the back reflection were monitored using an optical spectrum analyzer, while the RF signals for both were analyzed with RF spectrum analyzers utilizing two avalanche photodetectors (APDs). MSOs have been used for monitoring the output oscillations. Free-running laser dynamics is initially reported to function at a constant wavelength of λ = 1550 nm and a virtual laboratory temperature of T = 25 °C.

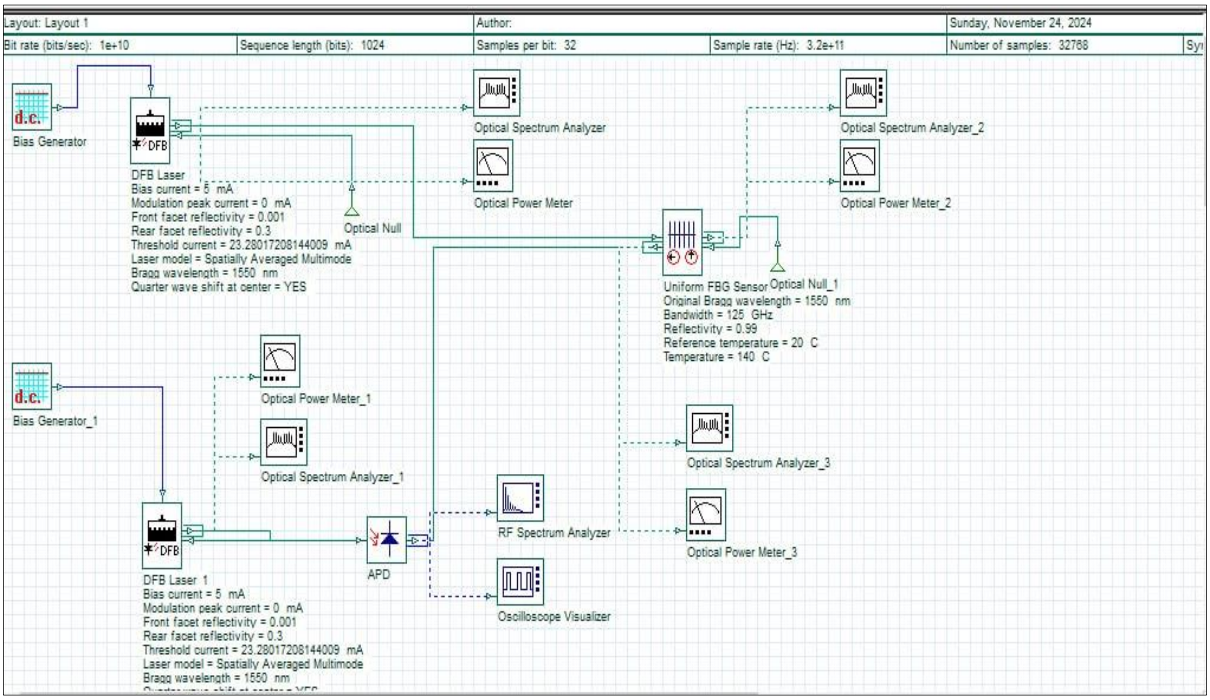

Fig. 2 Simulation configuration set-up for (SMI) using FBG.

Results and Discussion

Initially, the spectrum and properties of the free-running DFB, including the light-current (L-I) curve, are studied. Fig. 3 (A, B, C, D) illustrates the dynamics of a free-running DFB laser, which involves an optical spectrum analyzer (OSA), radio frequency (RF), time series, and phase space spectra, respectively. After considering self-mixing and temperature effects, this will be compared to the laser behavior. The OSA spectrum indicates that the laser exhibits an extended and broadened spectrum at 1550 nm, corresponding to a frequency of 5.8 GHz, with peak power amplitudes of 35.102 μW. Figure 3E presents the (L-I curve) of the solitary DFB LD at a temperature of 25°C and a wavelength of λ = 1550 nm. The figure shows that the DFB threshold current (I_{th}) is 17 mA. Below the threshold current, the output optical power exhibits a nearly linear increase with the input current before attaining the saturation region.

The primary focus of the self-mixing investigation is to treat the external target as a third mirror (FBG). By redirecting the laser into the resonant cavity, this reflective mirror changes the optical field within the laser cavity by affecting the reflectivity of the laser output mirror. Understanding the strength of the reflected feedback from the FBG to the laser cavity is crucial, as it interacts with the laser cavity modes. This is accomplished using Equation (6). By varying the temperature of the FBG and calculating the C value for each degree, it was found that C = 0.2, indicating that the self-mixing interference (SMI) operates in a weak feedback regime. Choosing the weak feedback was inevitable because using the FBG weakness, the back-reflected signal, and thus it is an important limitation for the SM. Although the DFB power at 27 mA has reached P = 1.1e-3 W, because we use the FBG as an external target, it is exposed to disturbance to achieve SMI. Because of the property of the FBG that it reflects a specific wavelength of the spectrum by reflection while transmitting the rest, and according to this principle, the signal power reflected from the FBG to the DFB ranges between 1.32e-4 W and 9.69e-7 W, which is a small amount compared to the original power of the DFB.

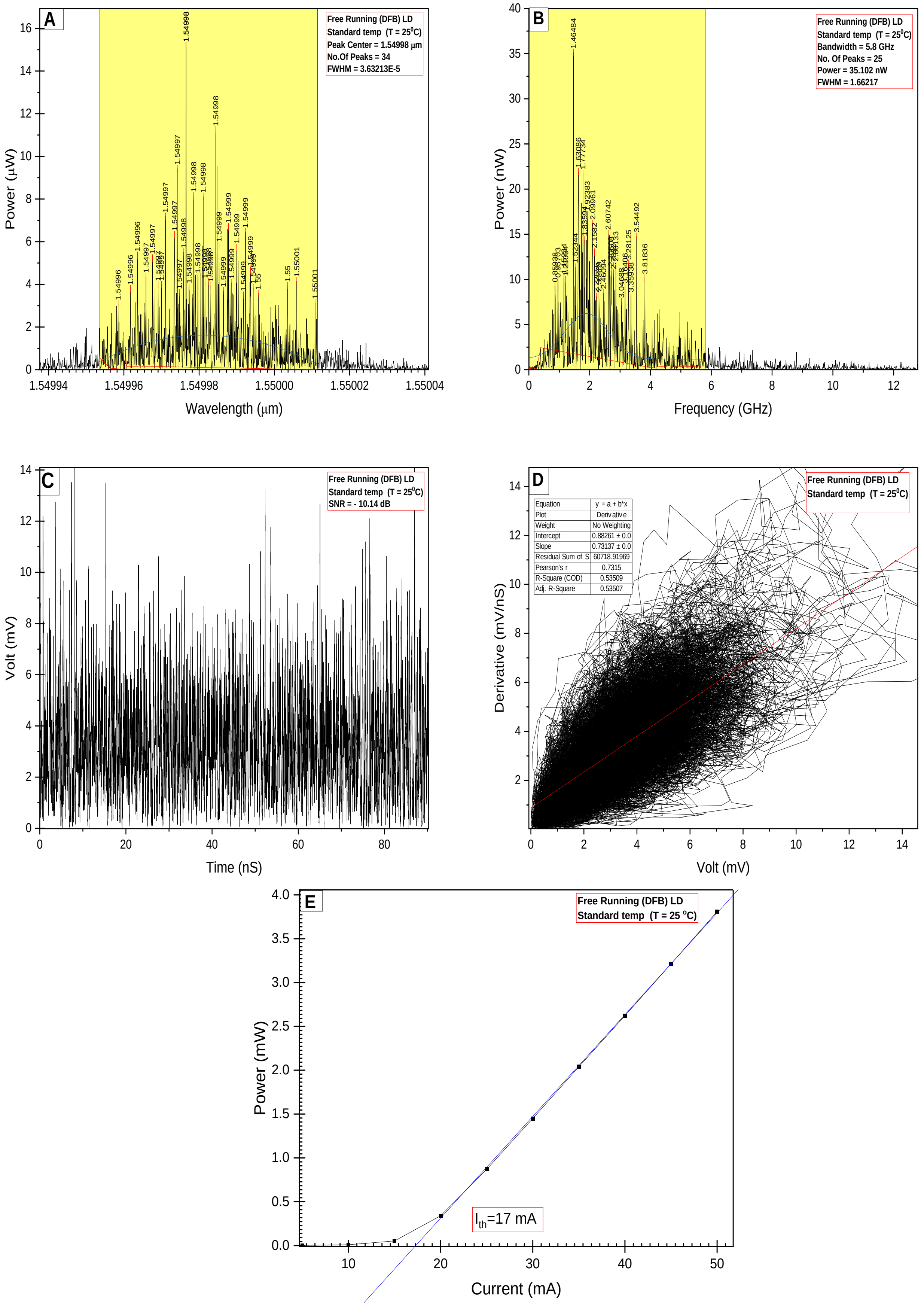

Fig. 3 Spectroscopy for free-running DFB laser with parameters λ =1550 nm, I = 27 mA, T = 25 °C. (A) Optical Spectrum Analyzer spectrum, (B) The Radio Frequency (RF) spectrum, (C) Time series, (D) Attractor, (E) L-I curve.

The system output waveform can be observed in Fig. 4 at different temperatures. At 30 °C, 50 °C, 80 °C, 90 °C, and 100 °C, the center wavelength is 1.500 µm, 1.5001 µm, 1.5002 µm, 1.5003 µm, and 1.5004 µm, respectively. The center of wavelength shifts with rising temperature; this has been proven in similar studies, such as Ref [31],[32],[33],[34].

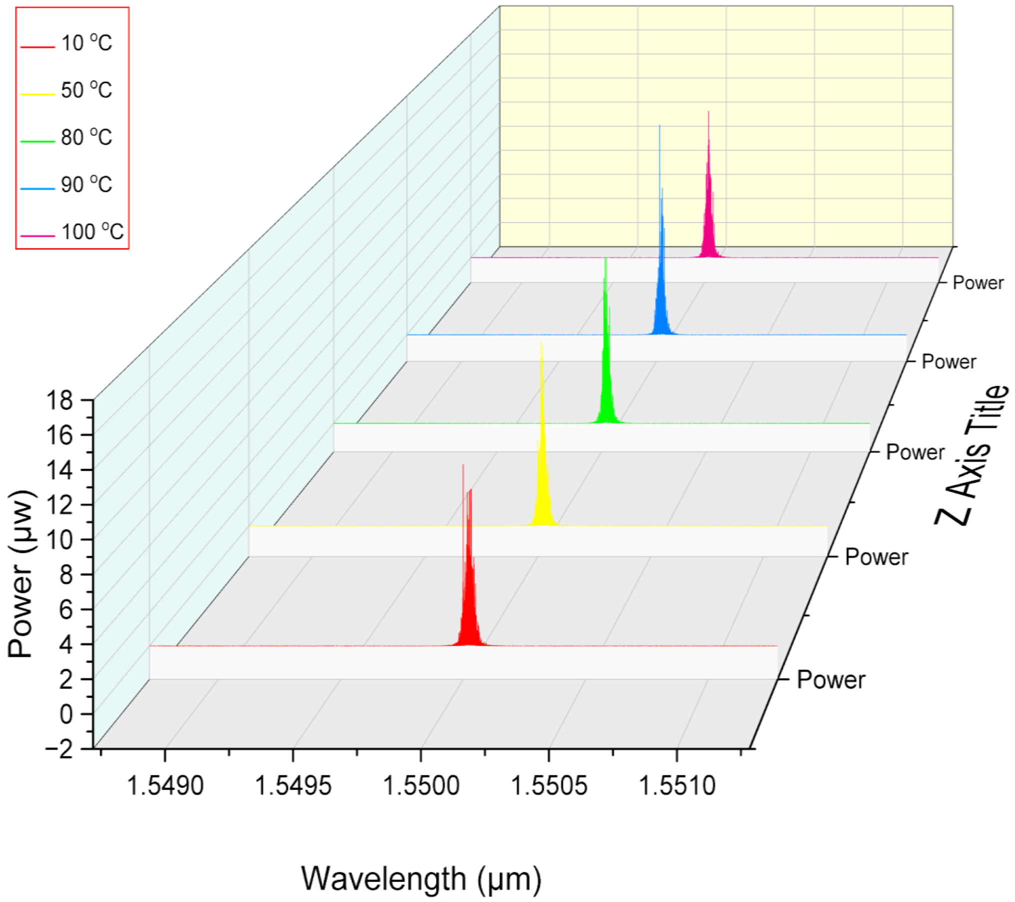

Fig. 4 Waveforms of the system output at various temperatures.

When the temperature externally fluctuates, the wavelength of the reflected light changes as well. Two primary variables affect this process: the optical fiber thermo-optic coefficient (ζ) and thermal expansion coefficient (α), where α = 0.55e-6 and ζ = 8.6e-6, respectively. Modifications in these factors affect the grating period and the effective refractive index of the waveguide. The wavelength shift in the FBG due to temperature variation ΔT can be described as follows [35]:

$$\frac{\Delta\lambda_B}{\lambda} = (\alpha + \zeta)\Delta T \dots\dots(8)$$

Fig. 5 shows a linear correlation between temperature and the system output waveform's center wavelength. A robust linear correlation occurs between the central wavelength shift and temperature fluctuations[36]. The characterization results reveal a 100 pm wavelength shift corresponding to each 10°C variation. The obtained sensitivity is 0.53 pm/°C. The high R-Square (COD) value confirms the effectiveness of the temperature change on the wavelength shift. As is known, the R value ranges between (0 to 1), and the closer the value is to 1, the more accurate the relationship between the two variables in this study. In this study, the R reached 0.95.

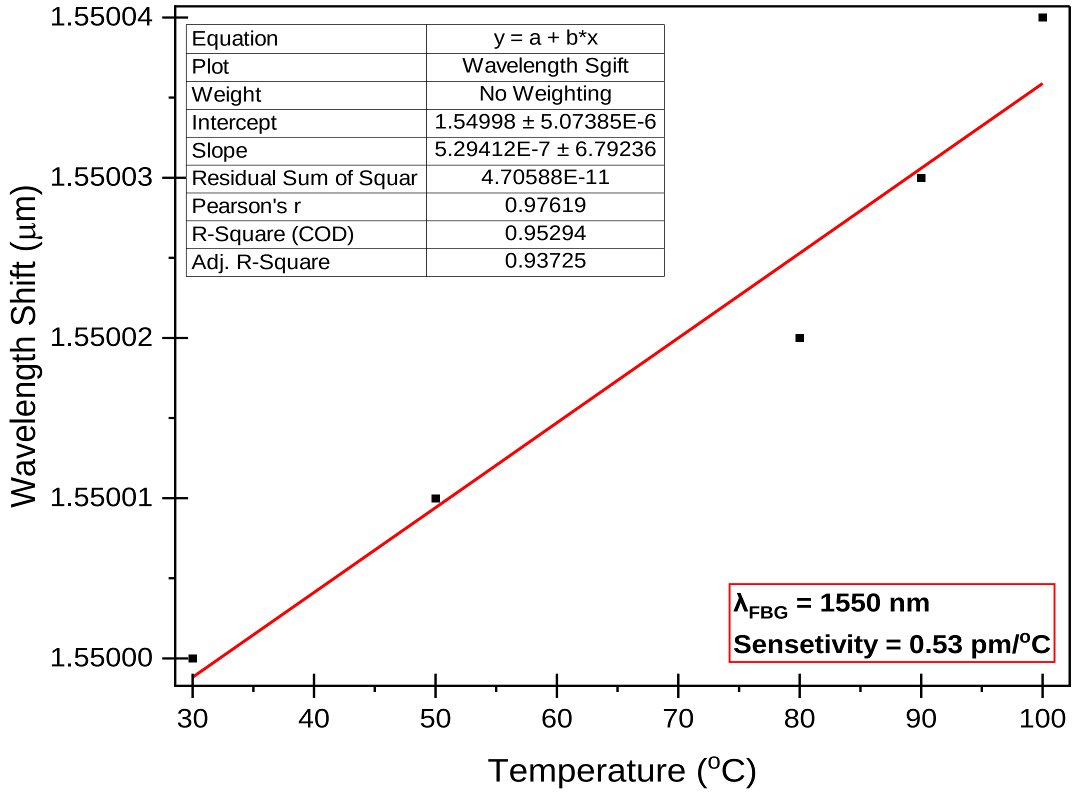

Fig. 5 Wavelength shift concerning the temperature applied to FBG.

Back to Fig. 1, which illustrates that RF spectrum analyzers and an oscilloscope were used to observe the electrical signals corresponding to the previously collected data. The signals were analyzed, leading to the emergence of frequency bandwidth, time sequence, and phase diagrams (Attractor) under different temperature circumstances as shown in Fig. 6. The figure clearly illustrates that the chaotic laser output state of the system varies significantly at various temperatures. At 30°C, the RF analysis can be observed, which shows that the chaotic BW has extended to be 8.1 GHz, and the number of spikes has doubled compared to the free-running situation. Additionally, the dynamics showed a decrease in the power for the spikes, with the highest mode reaching 19.5 nW. It can be observed clear spectral peaks when the laser output power goes up and down in a regular pattern, but when it behaves chaotically, there are no visible peaks, and the spectrum spreads out around the relaxation oscillation frequency [23],[37],[38].

When OFB strength ($k = 0.06$), at the same temperature, the voltage of the system varies as it progresses by its essential dynamics. By evaluating the signal-to-noise ratio (SNR), one can analyze and define the influence of self-mixing chaos on the resultant signal in terms of estimated noise. The signal-to-noise ratio (SNR) is calculated by dividing the data signal power by the noise power [39]. The results for the free-running DFB showed that the SNR value is -10.14 dB, but it decreased to -12.4 dB at 30°C. Also, the attractor graph, which represents the shape of infinite outward growth, is shown in the phase diagram. Analyzing attractor observation is necessary to accept chaotic systems and comprehend their future behavior. The system evolves toward an attractor, which includes a set of states, irrespective of the original conditions. This behavior is characterized as a strange attractor, a form of attractor caused by chaotic system dynamics. Assume that the strange attractor exhibits chaos and is sensitive to initial conditions. Therefore, any beginning points on the attractor that are infinitesimally close will eventually come together to form points that are likewise infinitesimally close after a specific number of iterations. After the same number of iterations, they will simultaneously separate away to produce points that are arbitrary distances apart (within the attractor's bounds). A dynamic system with a chaotic attractor is locally unstable yet globally stable. Following particular sequences that converge on the attractor, adjacent points separate from one another yet remain within the area around them [40]. The chaotic attractor at T = 30 °C is referred to as a strange

attractor because it differs greatly from other periodic attractors. Without crossing in phase space, the chaotic trajectory traverses a multidimensional space.
At 50 °C, the BW increases to 10.5 GHz, and the mode power increases substantially to 23 nW, compared to 19 nW at 30 °C. This increase confirms that the sensor detects a rise in the FBG temperature, which causes a wavelength shift. The SNR value decreases slightly for the same temperature, indicating a decrease in noise compared to the signal. As for the attractor, it continues with the same strange behavior that was mentioned previously.
At 80 °C, 90 °C, and 100 °C, Similar Behavior is observed in the behavior at 80 °C and 50 °C, as the bandwidth expands at 10 GHz, as well as the intensity of the pattern, but a difference is observed in the full width at half maximum (FWHM), values, as shown in Table No.2. However, the most notable attribute is the enhancement in SNR to (-8.37), representing the optimum level for signal-to-noise ratio. At 90 °C, the expansion in the BW starts to decrease, which is also what happens at 100 °C, but the SNR increases once more, indicating an elevation in noise relative to the signal.

Table 2. Statistics for chaotic dynamics changes against FBG assumed temperature.

	OSA			RF		
Temp °C	No. of Peaks	FWHM	Peak Center μm	No. of Peaks	FWHM GHz	Bandwidth GHz
0	49	3.16362E-5	1.55002	37	2.07052	8
10	47	2.36589E-5	1.55	23	2.17831	6.7
20	71	2.62484E-5	1.55002	36	2.86547	10.1
30	33	3.52651E-5	1.55	33	2.25469	8.1
40	50	3.85083E-5	1.55002	22	2.38023	7.91
50	36	3.50471E-5	1.55001	24	2.22415	10.5
60	35	2.39896E-5	1.55003	30	1.9229	11.4
70	38	3.23899E-5	1.55003	26	1.61887	10
80	46	3.71006E-5	1.55002	23	2.05849	10
90	29	3.6416E-5	1.55003	12	0.01032	9
100	45	2.99789E-5	1.55004	22	0.1759	7.18

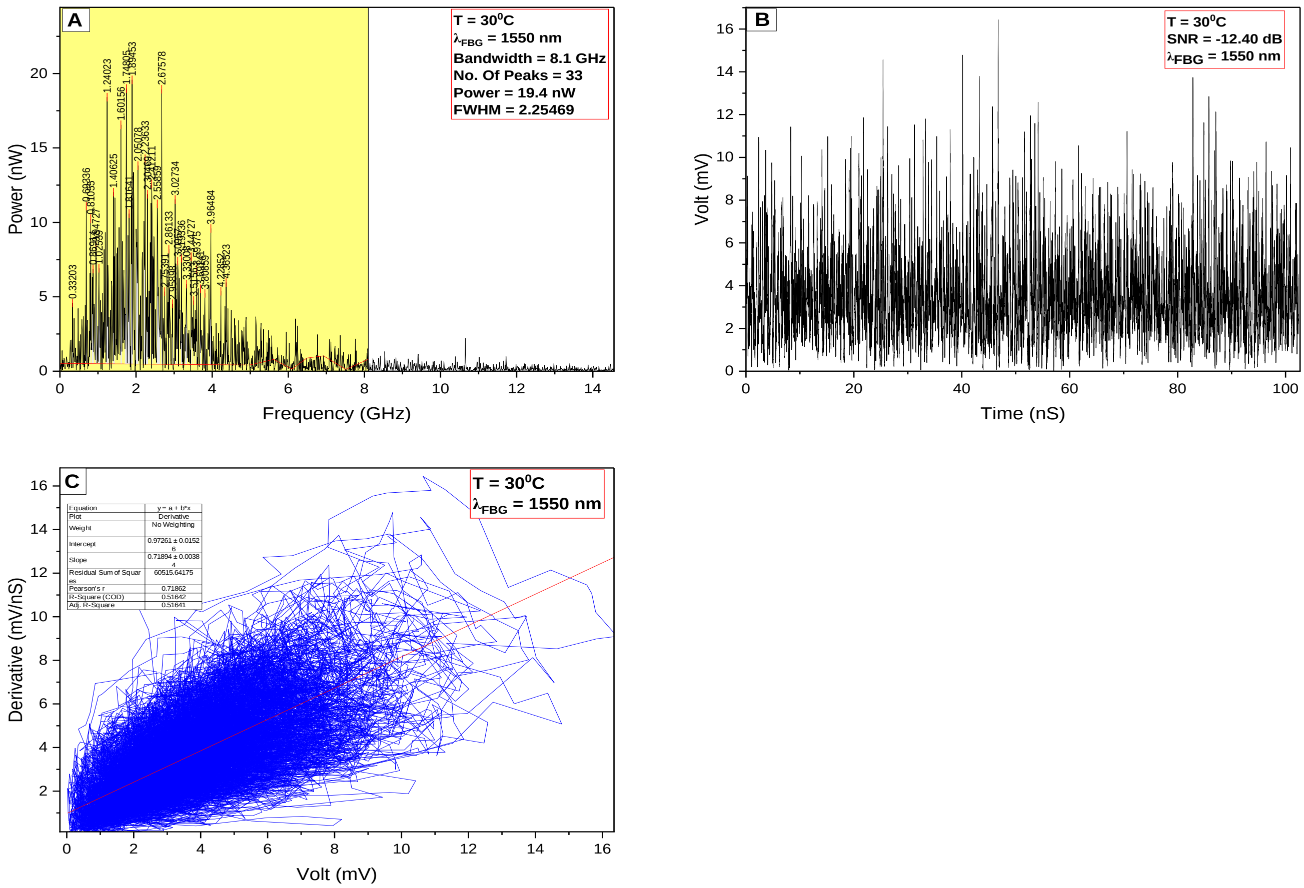

(1) Signal analysis at temperature 30°C.

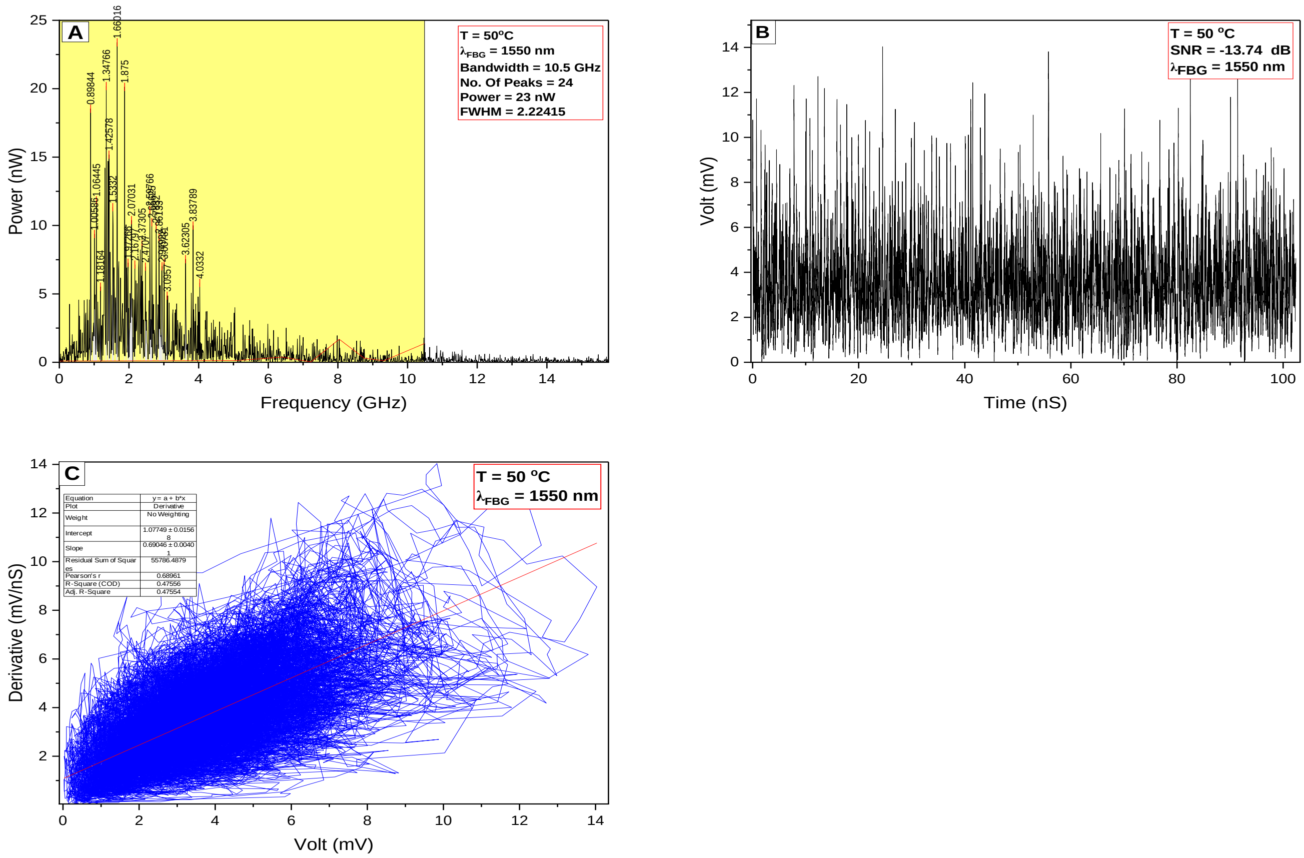

(2) Signal analysis at temperature 50°C.

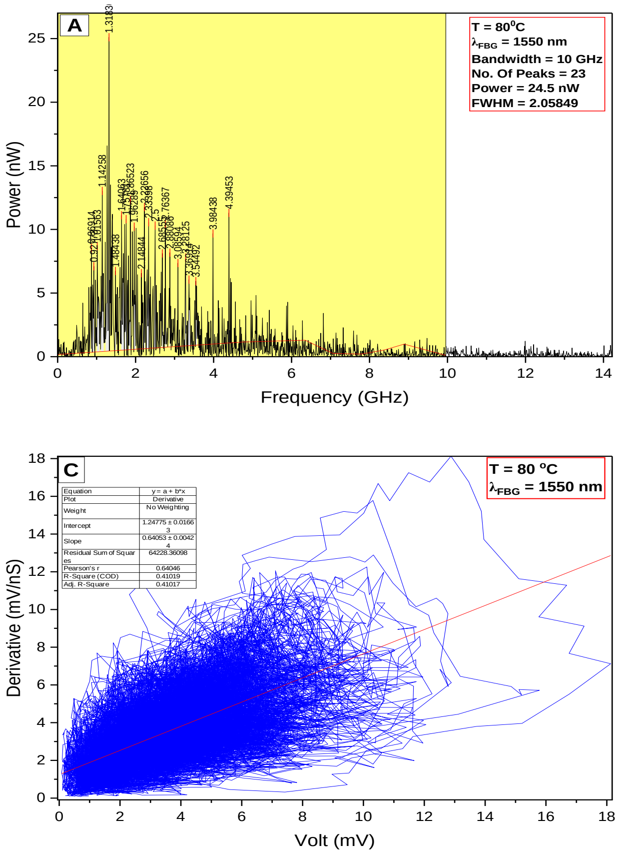

(3) Signal analysis at temperature 80°C.

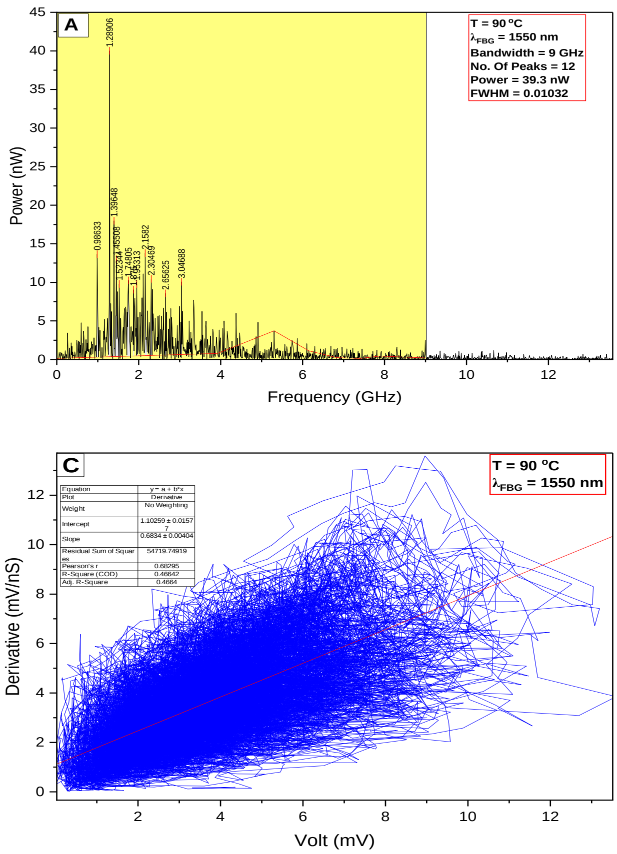

(4) Signal analysis at temperature 90°C.

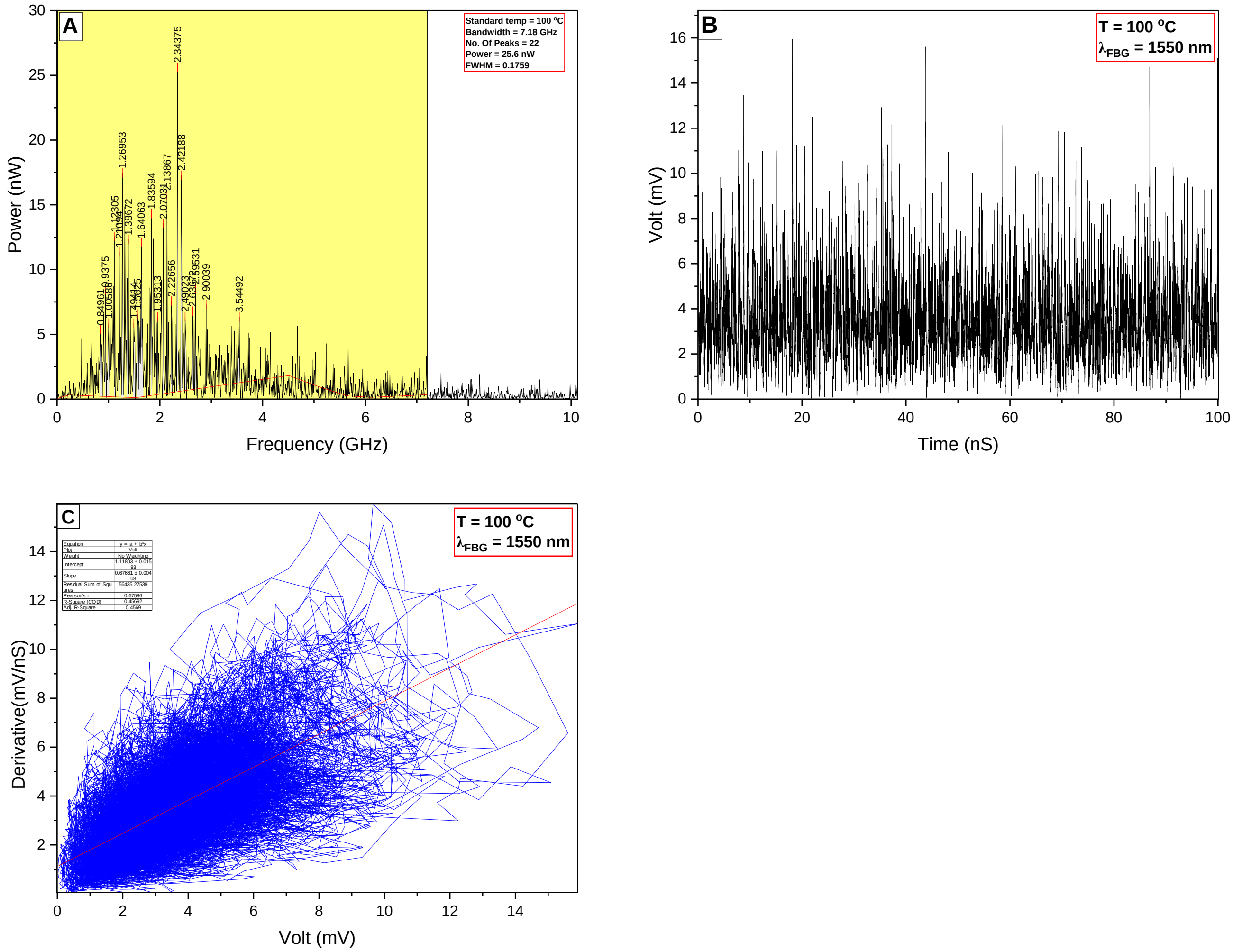

(5) Signal analysis at temperature 100°C.

Fig. 6. Signal analysis for different temperatures: (A) The RF power spectra (B) Time series (C) The attractor.

The effect of changing the FBG temperature is illustrated in Fig. 7 by the SMI bandwidth (FWHM) and the DFB feedback power level. The FWHM exhibits varying values as the temperature increases, and the change is asymmetric (Fig. 7A). On the other hand, the feedback power remains almost constant regardless of temperature changes. This effect occurs when only a small portion of the signal is reflected and interacts with the modes inside the laser cavity (Fig. 7B).

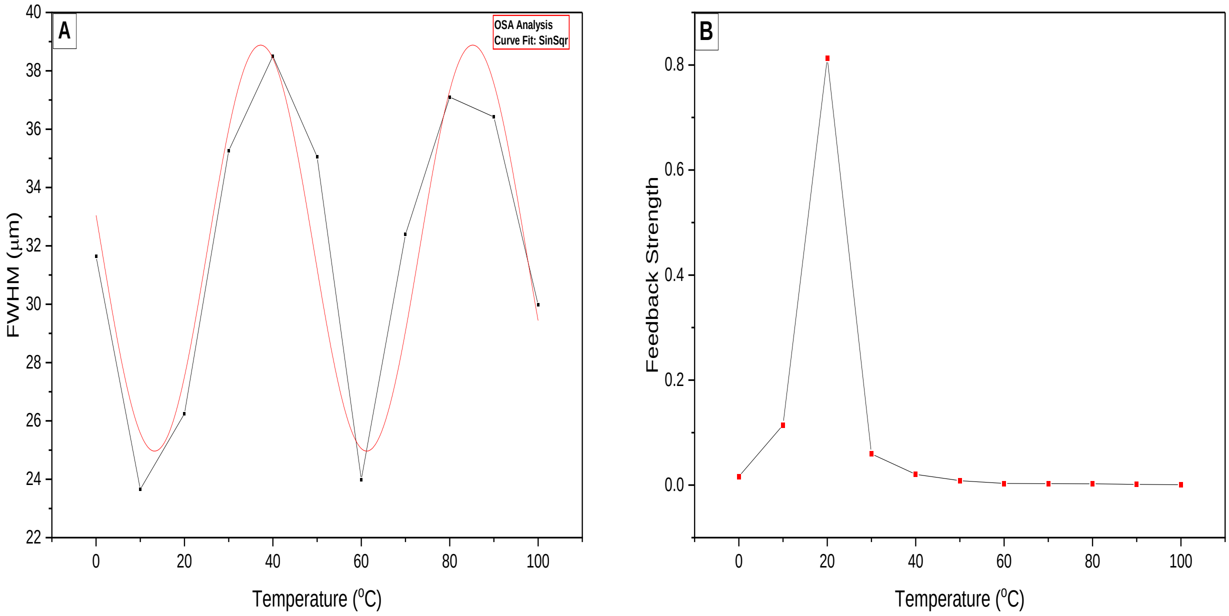

Fig. 7. The effect of temperature on: (A) FWHM, (B) Feedback Strength.

Conclusion

The simulation demonstrates the fiber optic sensor's potential for FBG interrogation by analyzing the self-mixing effect while it operates in a weak feedback regime. The evolution of the laser spectrum has been proven via observations in time, frequency, optical, and phase domains. This development was based on statistical analysis of the spectra, including wavelength shift, FWHM, number of peaks, and signal broadening (BW). According to the results, there is a strong linear relationship between temperature variations and the central wavelength shift. The characterization results show a wavelength shift of 100 µm for every 10°C change. The resulting sensitivity is 0.53 pm/°C. The results also show a bandwidth expansion to 11.4 GHz at 60 °C. Due to its uniqueness, temperature is the fundamental characteristic for all environments, and a chaotic system has a favorable effect on sensing. Therefore, it is intended to investigate the practical use of SMI further, utilizing several FBGs applied simultaneously. A fiber loop mirror with strong feedback will enable researchers to use this technique in applications such as those reported earlier and also in atmospheric layers sensing, particularly the troposphere layer.

Acknowledgements

The authors are grateful for the support of Mustansiriyah University, Baghdad, Iraq (www.uomustansiriyah.edu.iq).

References

[1] A. A. Siddiqui, U. Zabit, O. D. Bernal, G. Raja, and T. Bosch, "All Analog Processing of Speckle Affected Self-Mixing Interferometric Signals," *IEEE Sens J*, vol. 17, no. 18, pp. 5892–5899, Sep. 2017, doi: 10.1109/JSEN.2017.2737472.

[2] H. Wang, Y. Ruan, Y. Yu, Q. Guo, J. Xi, and J. Tong, "A New Algorithm for Displacement Measurement Using Self-Mixing Interferometry with Modulated Injection Current," *IEEE Access*, vol. 8, pp. 123253–123261, 2020, doi: 10.1109/ACCESS.2020.3007516.

[3] C. Bes, G. Plantier, and T. Bosch, "Displacement measurements using a self-mixing laser diode under moderate feedback," *IEEE Trans Instrum Meas*, vol. 55, no. 4, pp. 1101–1105, Aug. 2006, doi: 10.1109/TIM.2006.876544.

[4] M. Norgia, F. Bandi, A. Pesatori, and S. Donati, “High-sensitivity vibrometer based on FM self-mixing interferometry,” in *Journal of Physics: Conference Series*, Institute of Physics Publishing, Jun. 2019. doi: 10.1088/1742-6596/1249/1/012020.
[5] D. Tosi, “FBG/DFB-induced chaotic self-mixing analysis and sensing applications,” *Opt Laser Technol*, vol. 50, pp. 176–181, 2013, doi: 10.1016/j.optlastec.2013.02.020.
[6] Z. R. Ghayib and A. A. Hemed, “Simulating chaotic dynamics with variable polarisation of VCSEL twin lasers using FBG as a dynamic sensor,” *Pramana - Journal of Physics*, vol. 96, no. 2, Jun. 2022, doi: 10.1007/s12043-022-02305-2.
[7] F. A. Raghb and A. Hussain Dagher, “High Output Power Holmium-Doped Fiber Laser at 2100 nm,” 2024. [Online]. Available: https://mjpas.uomustansiriyah.edu.iq/index.php/mjpas
[8] A. A. Hemed, M. M. Fdhala, and S. M. Khorsheed, “Modified superstructure fiber Bragg grating for a filter application.”
[9] W. A. Jabbar, A. Hemed, M. Fadhala, and I. Al-Baidhany, “Characterization Study of DOUBLE Filtered Sensor Length Effect on Strain Sensitivity,” *East European Journal of Physics*, vol. 2023, no. 3, pp. 509–515, Sep. 2023, doi: 10.26565/2312-4334-2023-3-58.
[10] M. Suleiman, H. C. Seat and T. Bosch, "FBG-based dynamic strain sensors demodulated by self-mixing interferometry: Improving strain measurement resolution," 2009 IEEE Instrumentation and Measurement Technology Conference, Singapore, 2009, pp. 332-336, doi: 10.1109/IMTC.2009.5168470.
[11] N. A. Rosman, C. B. M. Rashidi, S. A. Aljunid, and R. Endut, “Temperature monitoring system using fiber Bragg grating (FBG) approach,” in *AIP Conference Proceedings*, American Institute of Physics Inc., Jan. 2020. doi: 10.1063/1.5142157.
[12] Taghreed Khalid Hameed, Wasmaa A. Jabbar, Zina Al_dagistany, Ayser A. Hemed, and Sami Salman Chiad, “Effect of FBG Fiber Dosimeter Division in Sensing Capability for Low Radiation Doses,” Journal of the College of Basic Education, vol. 30, no. 126, pp. 50–80, Oct. 2024, doi: 10.35950/cbej.v30i126.12226..
[13] T. Blanchet *et al.*, “Effect of radiation and temperature on high temperature resistant fiber Bragg gratings”, doi: 10.1117/12.2621473ï.
[14] Wasmaa A. Jabbar, “Simulating a Temperature, Stress And Strain FBG Sensor for Troposphere Layer,” *Int J Sci Res Sci Eng Technol*, vol. 11, no. 6, pp. 104–115, Nov. 2024, doi: 10.32628/IJSRSET2411617.
[15] D. Tosi, “Review of chirped fiber bragg grating (CFBG) fiber-optic sensors and their applications,” Jul. 04, 2018, *MDPI AG*. doi: 10.3390/s18072147.
[16] A. Cusano *et al.*, “Fiber Bragg Grating Sensors: Recent Advancements, Industrial Applications and Market Exploitation,” 2011.
[17] B. Liu *et al.*, “Laser self-mixing fiber bragg grating sensor for acoustic emission measurement,” *Sensors (Switzerland)*, vol. 18, no. 6, Jun. 2018, doi: 10.3390/s18061956.
[18] A. A. Hassan, Abdul Kareem H. Dagher, and Munther B. Hassan, “Initial Spot Size Influence of Hollow Gaussian Laser Beam on the Self-Focusing Phenomenon Inside Magnetized Plasma,” *Mustansiriyah Journal of Pure and Applied Sciences*, vol. 3, no. 2, pp. 32–40, Mar. 2025, doi: 10.47831/mjpas.v3i2.186.
[19] Moshe. Shapiro and Paul. Brumer, *Quantum control of molecular processes*. Wiley-VCH, 2012.
[20] A. AbdulHussain Hemed, “Optical Chaos Generation and Synchronization by Optical Ring Resonator,” 2016.
[21] Y. Yu, Y. Fan, B. Liu, Y. Yu, Y. Fan, and B. Liu, “Self-mixing interferometry and its applications,” 2016. [Online]. Available: https://ro.uow.edu.au/eispapers
[22] R. Lang and K. Kobayashi, “External Optical Feedback Effects on Semiconductor Injection Laser Properties,” 1980.
[23] Nie, Bairun, “Semiconductor laser dynamics induced by optical feedback for photonic microwave sensing,” 2023, University of Wollongong. Thesis. https://hdl.handle.net/10779/uow.27667896.v1.
[24] S. L. Chuang, “Physics of photonic devices,” 2nd edn. John Wiley & Sons, 2009.

[25] H. H. Khalaf and A. A. Hemed, “Effect of detuning in laser diode chaotic dynamics with unidirectional optical injection,” *Journal of Optics (India)*, 2025, doi: 10.1007/s12596-025-02509-w.
[26] G. Giuliani, M. Norgia, S. Donati, and T. Bosch, “Laser diode self-mixing technique for sensing applications,” 2002. [Online]. Available: http://iopscience.iop.org/1464-4258/4/6/371
[27] X. Wang, L. Lv, D. Zhu, H. Chen, and W. Huang, “Laser Self-Mixing Interferometer Based on Multiple Reflections and Phase-Modulation Technique,” *Photonics*, vol. 9, no. 6, Jun. 2022, doi: 10.3390/photonics9060430.
[28] T. Taimre and A. D. Rakić, “On the nature of Acket’s characteristic parameter C in semiconductor lasers,” *Appl Opt*, vol. 53, no. 5, p. 1001, Feb. 2014, doi: 10.1364/ao.53.001001.
[29] A. Arshad, U. Zabit, O. Bernal, C. Deleau, and R. Halir, “Robust integrated optical feedback interferometry via variable optical attenuation,” *Opt Express*, vol. 33, no. 8, p. 17566, Apr. 2025, doi: 10.1364/OE.550127.
[30] S. Chanu-Rigaldies, P. Lecomte, S. Ollivier, and T. Castelain, “Self-Mixing Interferometer for Acoustic Measurements through Vibrometric Calibration,” *Sensors*, vol. 24, no. 6, Mar. 2024, doi: 10.3390/s24061777.
[31] M. M. Elgaud, M. S. D. Zan, A. A. G. Abushagur and A. A. A. Bakar, "Analysis of independent strain-temperature fiber Bragg grating sensing technique using OptiSystem and OptiGrating," 2016 IEEE 6th International Conference on Photonics (ICP), Kuching, Malaysia, 2016, pp. 1-3, doi: 10.1109/ICP.2016.7510036.
[32] Z. Xie, W. Zeng, P. Li, H. Yan, and D. Han, “Thermal Modulation of a Chaotic Fiber Laser by Using a Phase-Shifted Fiber Bragg Grating,” *IEEE Photonics J*, vol. 15, no. 5, Oct. 2023, doi: 10.1109/JPHOT.2023.3302302.
[33] C. Molardi *et al.*, “Fiber Bragg Grating (FBG) sensors in a high-scattering optical fiber doped with MgO nanoparticles for polarization-dependent temperature sensing,” *Applied Sciences (Switzerland)*, vol. 9, no. 15, Aug. 2019, doi: 10.3390/app9153107.
[34] N. F. Naim *et al.*, “Design of High Performance Triangular Fiber Bragg Grating Temperature Sensor using OptiSystem and OptiGrating Software,” in *Journal of Physics: Conference Series*, Institute of Physics, 2023. doi: 10.1088/1742-6596/2627/1/012001.
[35] X. Zhao *et al.*, “Research Progress in Fiber Bragg Grating-Based Ocean Temperature and Depth Sensors,” Jan. 01, 2025, *Multidisciplinary Digital Publishing Institute (MDPI)*. doi: 10.3390/s25010183.
[36] B. A. Awad, A. L. Shuraiji, and R. J. Hassoon, “Design & simulation of fibre Bragg grating sensor for temperature and strain measurements,” in *AIP Conference Proceedings*, American Institute of Physics Inc., Dec. 2022. doi: 10.1063/5.0092585.
[37] X. Mu, Z. Yan, Y. Yu, H. Yan, and D. Han, “A tunable self-mixing chaotic laser based on high frequency electro-optic modulation,” *Opt Laser Technol*, vol. 127, Jul. 2020, doi: 10.1016/j.optlastec.2020.106172.
[38] M. Chai *et al.*, “Broadband chaos generation utilizing a wavelength-tunable monolithically integrated chaotic semiconductor laser subject to optical feedback,” *Opt Express*, vol. 30, no. 25, p. 44717, Dec. 2022, doi: 10.1364/oe.472708.
[39] R. Kieser, P. Reynisson, and T. J. Mulligan, “Definition of signal-to-noise ratio and its critical role in split-beam measurements,” *ICES Journal of Marine Science*, vol. 62, no. 1, pp. 123–130, Feb. 2005, doi: 10.1016/j.icesjms.2004.09.006.
[40] C. Grebogi, E. Ott, and J. A. Yorke, “Chaos, Strange Attractors, and Fractal Basin Boundaries in Nonlinear Dynamics,” 1987.